

Article

BaF(*p*-BDC)_{0.5} as the Catalyst Precursor for the Catalytic Dehydrochlorination of 1-Chloro-1,1-Difluoroethane to Vinylidene Fluoride

Shucheng Wang¹, Chuanzhao Wang², Houlin Yu², Wei Yu² , Yongnan Liu², Wucan Liu¹, Feixiang Zhou¹, Wanjin Yu¹, Jiuju Wang¹, Jianjun Zhang¹ and Wenfeng Han^{2,*} 

- ¹ State Key Laboratory of Fluorinated Greenhouse Gases Replacement and Control Treatment, Zhejiang Research Institute of Chemical Industry, Tianmushan Road 387, Hangzhou 310032, Zhejiang, China; wangshucheng1@sinochem.com (S.W.); liuwucan@sinochem.com (W.L.); zhoufeixiang01@sinochem.com (F.Z.); yuwanjin1@sinochem.com (W.Y.); wangjiuju@sinochem.com (J.W.); zhangjianjun@sinochem.com (J.Z.)
- ² Institute of Industrial Catalysis, Zhejiang University of Technology, Chaowang Road 18, Hangzhou 310014, Zhejiang, China; Wanglewcz555@163.com (C.W.); Yuhoulin88888@163.com (H.Y.); WillYmt1989@outlook.com (W.Y.); Yongnan_Liu@126.com (Y.L.)
- * Correspondence: hanwf@zjut.edu.cn



Citation: Wang, S.; Wang, C.; Yu, H.; Yu, W.; Liu, Y.; Liu, W.; Zhou, F.; Yu, W.; Wang, J.; Zhang, J.; et al. BaF(*p*-BDC)_{0.5} as the Catalyst Precursor for the Catalytic Dehydrochlorination of 1-Chloro-1,1-Difluoroethane to Vinylidene Fluoride. *Catalysts* **2021**, *11*, 1268. <https://doi.org/10.3390/catal11111268>

Academic Editors:
Peter Ramashadi Makgwane,
Naveen Kumar and
David E. Motaung

Received: 17 September 2021
Accepted: 18 October 2021
Published: 21 October 2021

Publisher's Note: MDPI stays neutral with regard to jurisdictional claims in published maps and institutional affiliations.



Copyright: © 2021 by the authors. Licensee MDPI, Basel, Switzerland. This article is an open access article distributed under the terms and conditions of the Creative Commons Attribution (CC BY) license (<https://creativecommons.org/licenses/by/4.0/>).

Abstract: A BaF(*p*-BDC)_{0.5} catalyst was prepared by solid state reaction at room temperature with Ba(OH)₂ as precursor, NH₄F as F source, and H₂(*p*-BDC) as organic ligand. The calcined samples were used as catalysts for dehydrochlorination of 1-chloro-1,1-difluoroethane to generate vinylidene fluoride (VDF) at 350 °C. Commercial production of VDF is carried out at 600–700 °C. Clearly, pyrolysis of the BaF(*p*-BDC)_{0.5} catalyst provided a promising way to prepare VDF at low temperatures. Prior to calcination, the activity of the BaF(*p*-BDC)_{0.5} catalyst was low. Following calcination at high temperatures, BaF(*p*-BDC)_{0.5} decomposed to BaF₂ and BaCO₃, and then the catalyst was chlorinated and fluorinated to BaClF, which showed high activity and stable VDF selectivity for dehydrochlorination of 1-Chloro-1,1-Difluoroethane to VDF.

Keywords: barium fluoride; catalytic pyrolysis; dehydrochlorination; 1-chloro-1,1-difluoroethane; vinylidene fluoride

1. Introduction

1,1-difluoroethylene (VDF) is a key monomer for the production of various resins, rubbers, and coatings [1,2]. Poly vinylidene fluorides (PVDF) prepared by VDF or co-polymers present chemical resistance, high temperature stability, oxidation resistance, weather resistance, piezoelectric, dielectric, and thermoelectric properties. Hence, they are widely applied in petrochemical, electronic, and electrical fields as well as fluorocarbon coatings. Recently, PVDF was confirmed to be promising material for the development of novel devices, such as sensors and electrolytes. Ferroelectric polymers function as prime candidates for sensors improving compactness and efficiency of the devices because of their multifunctionality [3,4]. PVDF is also one of the components in polymer electrolytes for sodium battery with high safety, suppression of sodium dendrite formation, and reduced electrolyte decomposition [5]. Consequently, the worldwide demand for VDF and PVDF is growing significantly. The production capacity ranks the second position among all the fluorinated polymers with 53,000 tons per year, only slightly lower than PTFE (Poly tetrafluoroethylene).

Although VDF can be produced via the dehydrofluorination of 1,1,1-trifluoroethane (HFC-143a) [6] or via simple co-pyrolysis of CHF₃ with CH₄ at elevated temperatures [7–9], the reaction conditions are rather harsh. Similarly, the co-pyrolysis of chlorodifluoromethane (HCFC-22) and methane also leads to the formation of VDF [10]. Although these routes

use inexpensive feedstocks, the yield and selectivity to VDF is low which are far from industrial application.

Currently, VDF is produced via the decomposition (dehydrochlorination) of HCFC-142b (1-Chloro-1,1-Difluoroethane) at high temperatures ($>650\text{ }^{\circ}\text{C}$) in the industry [1]. Unfortunately, due to the carbon deposition at elevated temperatures, the tube reactor tends to be blocked. Consequently, the reactor has to be cut off to remove coke, which significantly inhibits the efficiency of continuous production. Clearly, a catalyst which operates the pyrolysis of HCFC-142b at low temperatures is highly desired. Besides, efficient catalysts of dehydrochlorination also facilitate the preparation of other halogenated olefins, such as 1,1-dichloroethylene (VDC), vinyl chloride monomer (VCM), 2,3,3-tetrafluoropropylene (HFO-1234yf) [11–14].

For the reaction of HCFC-142b dehydrochlorination, the formation of extremely corrosive HCl and HF poses great challenge for the development of proper catalysts. Hence, the selection of catalysts materials is limited. Initially, we explored series of nitrogen doped carbon materials as the catalysts since they are inert to the corrosion of HCl and HF. It was found that the reaction temperature can be reduced from $650\text{ }^{\circ}\text{C}$ to $350\text{ }^{\circ}\text{C}$ in the presence of catalysts, which is beneficial to save energy and avoid coking in the reaction process [15,16]. Although N-doped activated carbon and mesoporous carbon exhibit moderate conversion and high selectivity to VDF, they are difficult to be recovered after coking and deactivation. Hence, it is still necessary to develop more effective catalysts to combine high catalytic performance and recyclability.

Therefore, we investigated series of metal fluorides, such as AlF_3 , SrF_2 , BaF_2 as the catalysts [17]. Among various metal fluorides, SrF_2 has high activity for cleavage of HCFC-142b to VDF, but its selectivity is low [18,19]. In addition, BaF_2 also shows high activity in this reaction, and the selectivity to VDF is 95% [20]. However, during the dehydrochlorination reaction, BaF_2 tends to be chlorinated by F species to BaClF under the reaction conditions [21]. If BaClF continues to be chlorinated to BaCl_2 , the conversion of HCFC-142b will be significantly reduced.

In this paper, the $\text{BaF}(p\text{-BDC})_{0.5}$ catalyst, barium fluoride connected with the framework of terephthalic acid was prepared via solid-state grinding at room temperature. The catalysts were calcined at different temperatures and the corresponding catalytic performance for the dehydrochlorination of 1-chloro-1,1-difluoroethane reaction over the catalysts were systematically evaluated.

2. Results

The catalytic performance of $\text{BaF}(p\text{-BDC})_{0.5}$ and the calcinated catalysts for the dehydrochlorination of 1-chloro-1,1-difluoroethane (CH_3CClF_2 , HCFC-142b) to vinylidene fluoride (VDF, $\text{CH}_2=\text{CF}_2$) under atmospheric pressure is illustrated in Figure 1. As depicted in Figure 1, the $\text{BaF}(p\text{-BDC})_{0.5}$ possesses poor activity for the dehydrochlorination of HCFC-142b with conversion lower than 10% and selectivity to VDF of about 82%. Following the calcination of $\text{BaF}(p\text{-BDC})_{0.5}$ at $500\text{ }^{\circ}\text{C}$, the activity of the catalyst ($\text{BaF}(p\text{-BDC})_{0.5}\text{-M500}$) is only slightly improved. By contrast, the selectivity to VDF is significantly improved, enhanced from 82 to 91%. After being calcinated at 600 and $700\text{ }^{\circ}\text{C}$, the activities of the catalysts ($\text{BaF}(p\text{-BDC})_{0.5}\text{-M600}$ and $\text{BaF}(p\text{-BDC})_{0.5}\text{-M700}$) are improved. The conversion of HCFC-142b is higher than 30% with selectivity to VDF higher than 90% which is significantly higher than BaF_2 or SrF_2 catalysts [18,19,21]. With further calcination at $800\text{ }^{\circ}\text{C}$, both the conversion of HCFC-142b and selectivity to VDF over the $\text{BaF}(p\text{-BDC})_{0.5}\text{-M800}$ are dramatically lower than that of $\text{BaF}(p\text{-BDC})_{0.5}\text{-M600}$ and $\text{BaF}(p\text{-BDC})_{0.5}\text{-M700}$. In addition, all the catalysts gradually deactivate after the induction period, and the selectivity to VDF is well maintained.

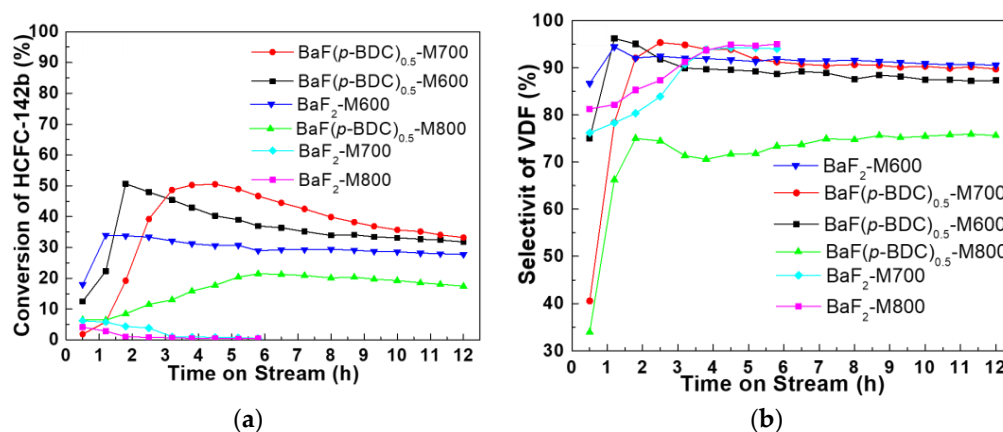


Figure 1. Catalytic performance of the $\text{BaF}(p\text{-BDC})_{0.5}$ catalysts for the pyrolysis of HCFC-142b as a function of time on stream at atmospheric pressure, a gas hourly space velocity (GHSV) of 1200 h^{-1} , and a reaction temperature of $350 \text{ }^\circ\text{C}$. (a) Conversion of HCFC-142b, (b) Selectivity to vinylidene fluoride (VDF).

As mentioned in our previous study [15,21], for BaF_2 , the reason for deactivation during dehydrochlorination is that the catalyst reacts with HCl generated in the reaction, and then the element F on the catalyst is further replaced by Cl. In addition to carbon deposition, this is the main cause of deactivation. It is worth noting that the effect of carbon deposition on the activity of the catalyst was minor within the time on stream investigated. Calcination of BaF_2 is a simple method to reduce its deactivation. However, it is very sensitive for BaF_2 calcinated at high temperatures, and its activity is greatly reduced due to obvious sintering when calcined at above $600 \text{ }^\circ\text{C}$ (Figure 1a). Different from BaF_2 prepared by precipitation, BaF_2 obtained by calcination and decomposition of $\text{BaF}(p\text{-BDC})_{0.5}$ exhibits enhanced catalytic performance.

Clearly, $\text{BaF}(p\text{-BDC})_{0.5}$ presents promising catalytic performance for the dehydrochlorination reaction. The doping of $p\text{-BDC}$ to BaF_2 plays a positive role in the catalytic activity. Hence, the catalysts were characterized in detail. Determined by N_2 adsorption and desorption, the specific surface areas of all catalyst samples are rather low ($<1 \text{ m}^2/\text{g}$). We suggest that the specific surface play a minor role in the performance differences of catalysts.

$\text{BaF}(p\text{-BDC})_{0.5}$ was facilely prepared by solid state reaction of $\text{Ba}(\text{OH})_2 \cdot 8\text{H}_2\text{O}$ with $\text{NH}_4\text{F}/\text{PTA}$ at room temperature [22]. As shown in Figure 2a, the XRD spectrum of $\text{BaF}(p\text{-BDC})_{0.5}$ agrees well with the report of Breinfeld [22]. Clearly, $\text{BaF}(p\text{-BDC})_{0.5}$ was achieved successfully. Following calcination at $500 \text{ }^\circ\text{C}$, the intensities of diffraction peak are enhanced. However, no other new impurities are identified in Figure 2a. However, when the calcination temperature was increased to $600 \text{ }^\circ\text{C}$, as shown in Figure 2b, the specific diffraction peaks assigned to $\text{BaF}(p\text{-BDC})_{0.5}$ disappears, and instead, the characteristic peaks ascribed to BaCO_3 and BaF_2 are presented. Moreover, elevated calcination temperature facilitates the complete decomposition of $\text{BaF}(p\text{-BDC})_{0.5}$ to BaCO_3 and BaF_2 , as well as the interaction between BaCO_3 and BaF_2 , which means that the initial activity of the $\text{BaF}(p\text{-BDC})_{0.5}\text{-M600}$, $\text{BaF}(p\text{-BDC})_{0.5}\text{-M700}$, and $\text{BaF}(p\text{-BDC})_{0.5}\text{-M800}$ catalysts (Figure 1) originated from the synergistic effect of BaCO_3 and BaF_2 .

With $\text{BaF}(p\text{-BDC})_{0.5}\text{-M600}$, $\text{BaF}(p\text{-BDC})_{0.5}\text{-M700}$ and $\text{BaF}(p\text{-BDC})_{0.5}\text{-M800}$ as catalysts, there exists an induction period (Figure 1). In order to clarify the true active species for dehydrochlorination, $\text{BaF}(p\text{-BDC})_{0.5}\text{-M600}$ samples with different reaction time were selected, and the XRD patterns are shown in Figure 2c. After time on stream of 2 h, the catalyst exhibits the highest activity, and the phase of the catalyst is composed of pure BaClF , which confirms that BaClF is the efficient component for the reaction [21]. Following the reaction time extends from 2 to 12 h, the conversion of HCFC-142b declines from 50 to 38%, and meantime, the phase of the catalyst changes from pure BaClF to the mixture of BaClF and BaCl_2 . As reported previously, BaCl_2 presents low activity for dehydrochlorination. As a result, it is

suggested that the increase in activity is ascribed to the fluorination as well as chlorination of BaF_2 and BaCO_3 to BaClF , while BaClF is inevitable to be further chlorinated to BaCl_2 , leading to the decrease in activity. In addition, the XRD diffraction of used $\text{BaF}(p\text{-BDC})_{0.5}\text{-M700}$ and $\text{BaF}(p\text{-BDC})_{0.5}\text{-M800}$ further reinforces the conclusion. As shown in Figure 2d, after time on stream of 12 h, the characteristic peak attributed to BaCl_2 could be found in the catalysts, but the diffraction intensity of used $\text{BaF}(p\text{-BDC})_{0.5}\text{-M800}$ is much weaker.

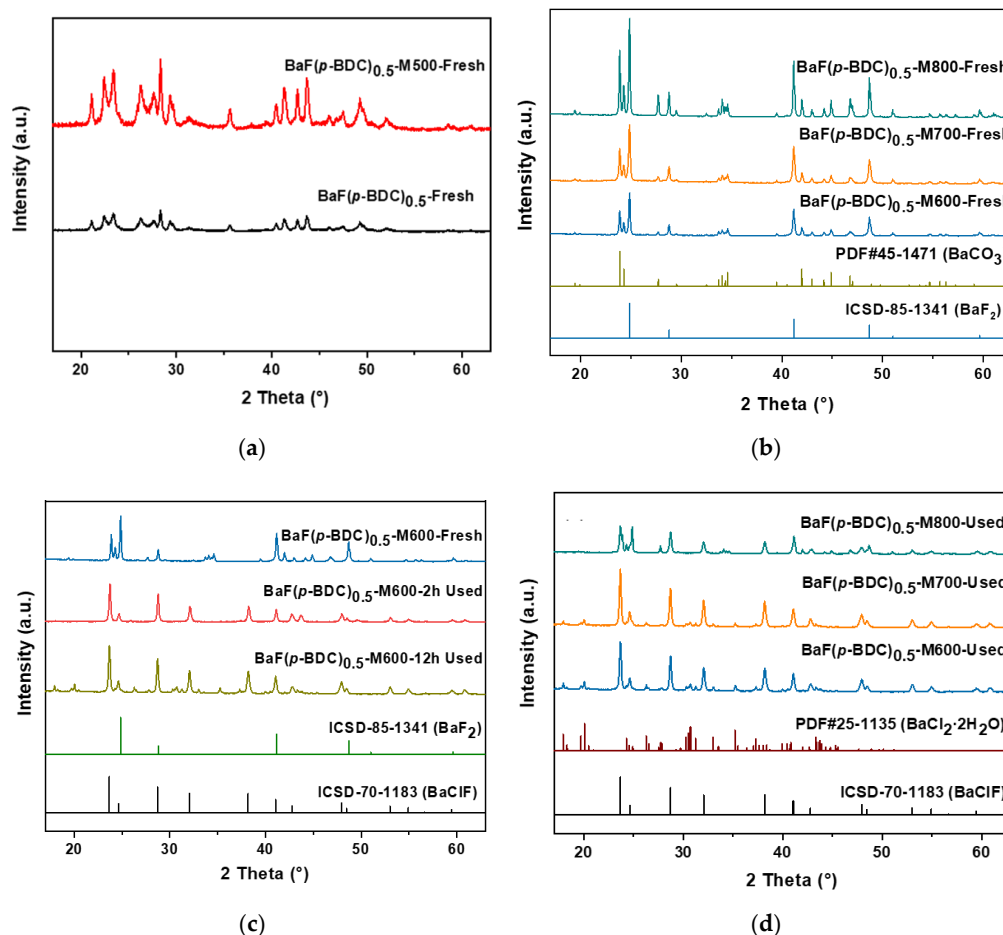


Figure 2. XRD patterns of fresh (a,b) and used catalysts (c,d), respectively.

The obtained catalysts were further investigated by XPS (Figure 3). It is noticed that the binding energy of $\text{Ba } 3d_{5/2}$ in $\text{BaF}(p\text{-DC})_{0.5}$ decreases by 0.4 eV following calcination from 400 to 600 °C. The binding energy of $\text{Ba } 3d_{5/2}$ in $\text{BaF}(p\text{-BDC})_{0.5}\text{-M600}$, $\text{BaF}(p\text{-BDC})_{0.5}\text{-M700}$ and $\text{BaF}(p\text{-BDC})_{0.5}\text{-M800}$ are all around 779.80 eV, which is the typical binding energy of $\text{Ba } 3d_{5/2}$ in BaF_2 and BaCO_3 [23]. Combined with the activity diagram and XRD characterization of the catalyst, it could be confirmed that $\text{BaF}(p\text{-BDC})_{0.5}$ gradually decomposes after calcination at 400–600 °C, and could be completely decomposed to BaCO_3 and BaF_2 at 600 °C. In addition, the shift of $\text{Ba } 3d_{5/2}$ binding energy indicates the strong interaction between Ba and carbon residuals derived from the decomposition of $p\text{-BDC}$. Clearly, this interaction contributes to the improvement of catalytic activity and stability [18].

Figure 4 exhibited the SEM images of the calcinated catalysts. For $\text{BaF}(p\text{-BDC})_{0.5}\text{-M500}$, irregular particles were obtained after calcination. The average size of the catalyst is ca. 500 nm. With the increase in calcination temperature, the size of the grains becomes more uneven but are still accompanied with small particles. With the calcination temperature being increased to 700 °C, the particle size aggregated up to 2 μm . Meantime, the particles turn more dense, indicating the occurrence of sintering. As expected, with further increase in calcination temperature to 800 °C, larger particles could be obtained. Then, it is

reasonable to deduce that the inferior catalytic performance of $\text{BaF}(p\text{-BDC})_{0.5}\text{-M700}$ and $\text{BaF}(p\text{-BDC})_{0.5}\text{-M800}$ compared with $\text{BaF}(p\text{-BDC})_{0.5}\text{-M600}$ results from the larger grain size.

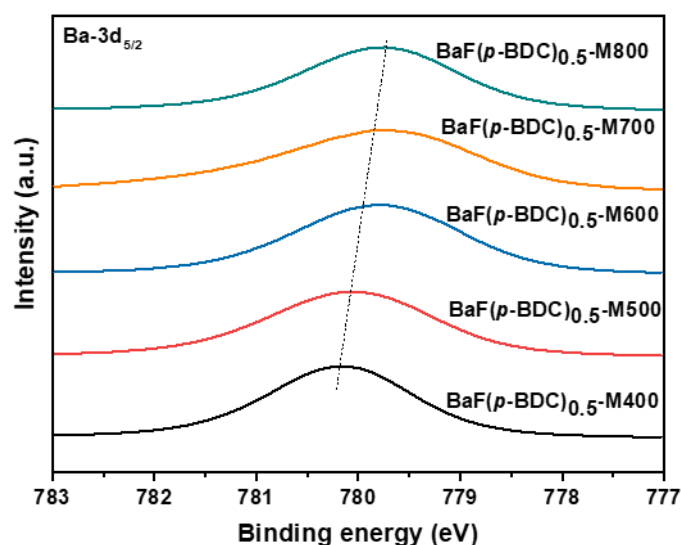


Figure 3. Ba 3d XPS spectra of calcinated $\text{BaF}(p\text{-BDC})_{0.5}$ catalysts.

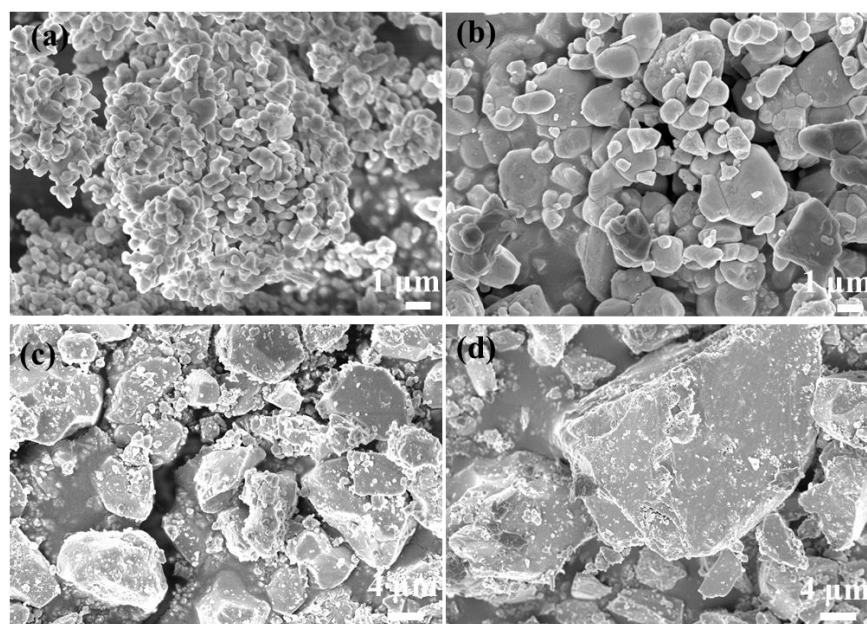


Figure 4. SEM images of (a) $\text{BaF}(p\text{-BDC})_{0.5}\text{-M500}$, (b) $\text{BaF}(p\text{-BDC})_{0.5}\text{-M600}$, (c) $\text{BaF}(p\text{-BDC})_{0.5}\text{-M700}$, (d) $\text{BaF}(p\text{-BDC})_{0.5}\text{-M800}$. The scale bar of (a–d) are 1 μm , 1 μm , 4 μm and 4 μm , respectively.

Before the reaction, the average grain sizes of $\text{BaF}(p\text{-BDC})_{0.5}\text{-M600}$, $\text{BaF}(p\text{-BDC})_{0.5}\text{-M700}$ and $\text{BaF}(p\text{-BDC})_{0.5}\text{-M800}$ were 82.5, 116.1, and 164.5 nm, respectively. After the reaction, the grain size of the specific catalysts were 159.4, 191.4, and 257.9 nm, respectively. After 2 h of reaction, the $\text{BaF}(p\text{-BDC})_{0.5}\text{-M600}$ was composed by BaClF , with a grain size of 55.1 nm. After 12 h of reaction, the grain size of $\text{BaF}(p\text{-BDC})_{0.5}\text{-M600}$ (BaClF) is 159.4 nm (Figure 5). Clearly, the grain size of the catalyst increases significantly.

In order to further verify the effect of crystal size on the catalytic performance, the crystal size of fresh and used catalysts calcinated at 400–800 $^{\circ}\text{C}$ are compared. The crystal sizes are determined by the Scherrer equation based on XRD [24].

The crystal sizes of $\text{BaF}(p\text{-BDC})_{0.5}$ catalysts calcined in air at 400, 500, 600, 700, and 800 $^{\circ}\text{C}$ are illustrated in Figure 6. Before the reaction, the crystal sizes of $\text{BaF}(p\text{-BDC})_{0.5}$

calcined at different temperatures are 21.8, 43.0, 82.5, 116.1, and 164.5 nm, respectively. After reaction, the crystal sizes of the catalyst are 29.4, 53.8, 159.4, 191.4, and 257.9 nm, respectively. It is found that the higher the calcination temperature is, the more serious the sintering is. Low calcination temperature of $\text{BaF}(p\text{-BDC})_{0.5}$ is beneficial to the disordered structure of $\text{BaF}(p\text{-BDC})_{0.5}$. By comparing the crystal size of the catalyst before and after the reaction, although the reaction was carried out at 350 °C, it is found that the crystal size of the catalyst increases significantly, and its influence is more significant than that of calcination at high temperatures. This indicates that the crystal size of the catalyst increases obviously when the catalyst is chlorinated during the reaction, which indicates that the structure and phase state of the catalyst have changed significantly.

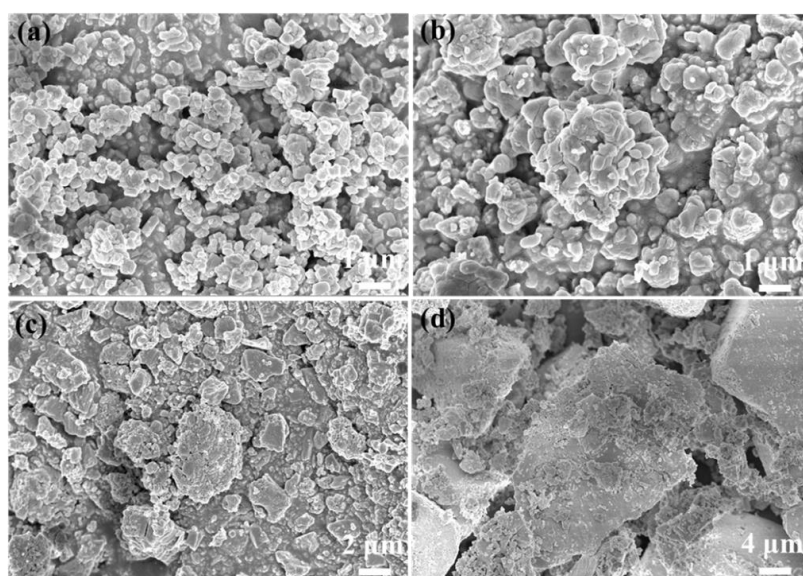


Figure 5. SEM images of (a) spent $\text{BaF}(p\text{-BDC})_{0.5}\text{-M500}$, (b) spent $\text{BaF}(p\text{-BDC})_{0.5}\text{-M600}$, (c) spent $\text{BaF}(p\text{-BDC})_{0.5}\text{-M700}$, (d) spent $\text{BaF}(p\text{-BDC})_{0.5}\text{-M800}$. The scale bar of (a–d) are 1 μm , 1 μm , 2 μm and 4 μm , respectively.

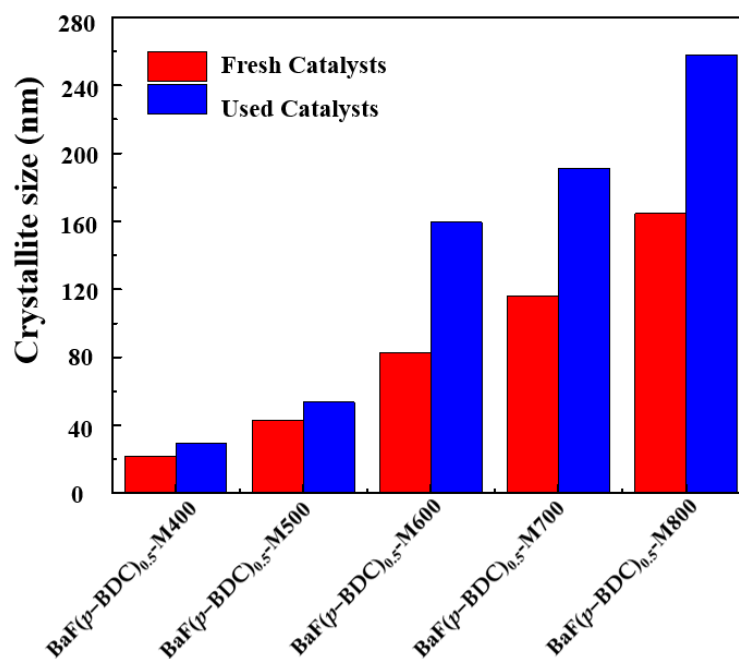


Figure 6. The crystal size of fresh and used catalysts.

As indicated in Figure 2b, BaCO_3 is derived during the calcination of $\text{BaF}(p\text{-BDC})_{0.5}$. To elucidate the synergism of BaCO_3 to the BaF_2 catalyst, additional experiments were carried out. Through combining the results of XRD and XPS, it could evidence that the composition of the $\text{BaF}(p\text{-BDC})_{0.5}\text{-M600}$ is BaF_2 and BaCO_3 . Then, in order to understand the synergism between BaCO_3 and BaF_2 , the catalytic activities were compared for BaCO_3 annealed at $600\text{ }^\circ\text{C}$ ($\text{BaCO}_3\text{-M600}$), BaF_2 ($\text{BaF}_2\text{-M600}$) and $\text{BaF}(p\text{-BDC})_{0.5}\text{-M600}$. As shown in Figure 7, the HCFC-142b conversion over $\text{BaF}_2\text{-M600}$ was the lowest, but the selectivity to VDF is high. By contrast, $\text{BaCO}_3\text{-M600}$ exhibits higher activity for HCFC-142b conversion, but the selectivity of VDF is lower than $\text{BaF}_2\text{-M600}$. Then, as expected, $\text{BaF}(p\text{-BDC})_{0.5}\text{-M600}$ constituted by BaCO_3 and BaF_2 , could maintain the merits of BaCO_3 and BaF_2 exhibiting relatively high HCFC-142 conversion and VDF selectivity. Besides, from Figure 2c, we suggest that the active species of $\text{BaF}(p\text{-BDC})_{0.5}\text{-M600}$ was BaClF . However, the pure BaClF calcinated at $600\text{ }^\circ\text{C}$ (BaClF-M600) shows lower activity than $\text{BaF}(p\text{-BDC})_{0.5}\text{-M600}$, which could further support the cooperation between BaCO_3 and BaF_2 . The change of BaF_2 during the reaction was investigated by our previous report [21], BaF_2 was confirmed to be turned into BaCl_2 leading to the deactivation of the catalysts. The transformation process of BaCO_3 is identical with BaF_2 (Figure 7c,d) as well as $\text{BaF}(p\text{-BDC})_{0.5}\text{-M600}$.

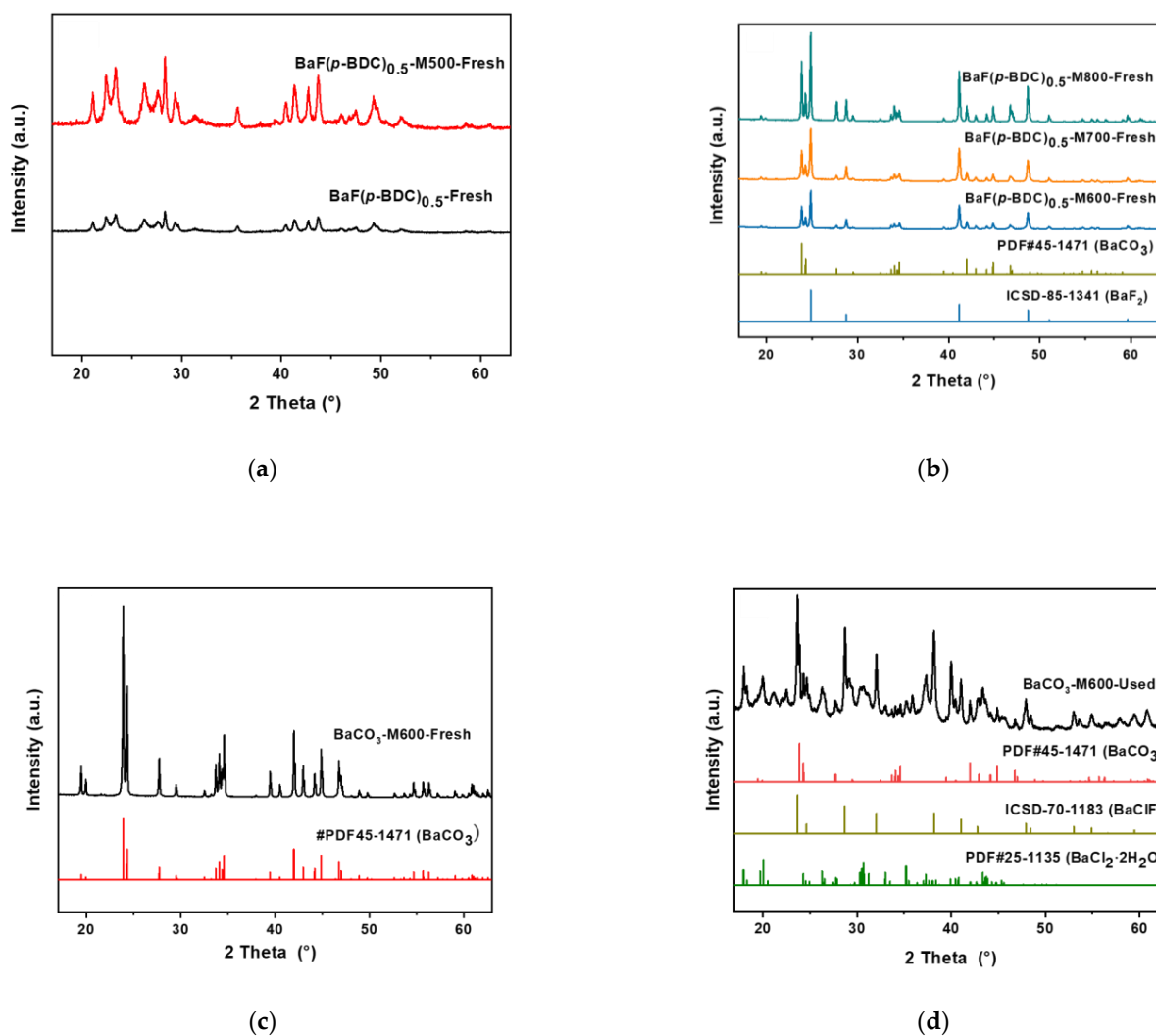


Figure 7. Catalytic performance of $\text{BaF}(p\text{-BDC})_{0.5}\text{-M600}$, $\text{BaF}_2\text{-M600}$, $\text{BaCO}_3\text{-M600}$, and BaClF-M600 catalysts for the dechlorination of HCFC-142b as a function of time on stream at atmospheric pressure, a gas hourly space velocity (GHSV) of 1200 h^{-1} , and a reaction temperature of $350\text{ }^\circ\text{C}$. (a) Conversion of HCFC-142b, (b) Selectivity to vinylidene fluoride (VDF); XRD patterns of fresh (c) and used BaCO_3 catalysts (d).

3. Materials and Methods

3.1. Preparation of Catalysts

Ba(OH)₂·8H₂O and NH₄F were selected as Ba and F sources, respectively. PTA (terephthalic acid) was adopted as organic ligands. Firstly, 0.05 mol NH₄F and 0.025 mol PTA were added to the mortar rigorously for 0.5 h. Afterward, 0.05 mol Ba(OH)₂·8H₂O powder was added to the above mixture with grinding for another 1 h. Within the reaction of the mixture, NH₃ was generated and crystal water released. Then, the mixture was treated under 110 °C for 5 h to produce the BaF(*p*-BDC)_{0.5}. It is to be noted that all the raw materials were obtained from Aladdin Co. (Shanghai, China) without further purification. Then the samples were calcined in a muffle furnace at different temperatures (400~800 °C) for 5 h to obtain the catalyst; they were recorded as BaF(*p*-BDC)_{0.5}-M400, BaF(*p*-BDC)_{0.5}-M500, BaF(*p*-BDC)_{0.5}-M600, BaF(*p*-BDC)_{0.5}-M700 and BaF(*p*-BDC)_{0.5}-M800. In addition, the reagents used in the work were all get from Aladdin, Shanghai, China without other treatment.

3.2. Catalytic Activity

The catalytic activity evaluation was conducted in a fixed-bed reactor (i.d. = 22 mm). Firstly, the prepared Ba-based catalysts (2 mL) was loaded to the isothermal zone of the reactor. Then, the mixture of HCFC-142b (20 mL min⁻¹) and N₂ (20 mL min⁻¹) was introduced to the reactor, accordingly. The gas hourly space velocity (GHSV) was maintained at 1200 h⁻¹. The reactions were carried out at 350 °C, and the reaction temperature of the catalysts layer was confirmed by inserting a thermal couple into the middle of the catalyst bed. Owing to the outlet gases possibly containing HCl and HF, KOH solution (1 mol/L) was used to remove the acid gas. A gas chromatograph (GC-1690 JieDao, Hangzhou, China) equipped with a thermal conductivity detector (TCD, Hangzhou, China) was used to analyze the gas composition. As noted, blank experiments showed that no VF was detected without catalysts at 350 °C.

3.3. Catalyst Characterization

The phase compositions of the synthesized catalysts were confirmed by X-ray diffraction (XRD) experiments, performed with the X'Pert Pro analytical instrument (Almelo, Overijssel, The Netherlands). The chemical states of Ba species were analyzed via X-Ray photoelectron spectroscopy (XPS) spectra, conducted on the Thermo EscaLab 250Xi (Cambridge, Waltham, MA, USA), equipped with monochromatized Al K α X-ray (1486.6 eV). The binding energy values were corrected by C1s line at 284.5 eV. The morphologies of the Ba-based catalysts were obtained by scanning electron microscopy (SEM), carried out with Helios G4 CX (Cambridge, Waltham, MA, USA).

4. Conclusions

BaF(*p*-BDC)_{0.5} catalysts were successfully prepared via the solid-state reaction method at room temperature. BaF₂ and BaCO₃ were obtained after calcination at high temperature, which promotes the pyrolysis of HCFC-142b (CH₃CClF₂) to VDF (CH₂=CF₂) at 350 °C. The reaction temperature was significantly lower than the industrial manufacturing temperature (600–700 °C) by the thermal decomposition of HCFC-142b. In the reaction, BaF₂ and BaCO₃ were chlorinated to BaClF, which is the active species in this reaction. The pyrolysis of BaF(*p*-BDC)_{0.5} forms the mixture of BaF₂ and BaCO₃ and then BaClF with small crystal size was derived during the reaction, exhibiting high activity for dehydrochlorination of HCFC-142b.

Author Contributions: Conceptualization, W.H.; methodology, W.H.; formal analysis, C.W. and H.Y.; investigation, C.W., H.Y., W.Y. (Wei Yu) and Y.L.; resources, S.W.; data curation, C.W., H.Y., W.Y. (Wei Yu), F.Z., W.Y. (Wanjin Yu), J.W. and Y.L.; writing—original draft preparation, W.Y. (Wei Yu) and W.H.; writing—review and editing, W.H.; supervision, W.H., W.L. and J.Z.; project administration, W.H.; funding acquisition, W.H., W.L. and J.Z. All authors have read and agreed to the published version of the manuscript.

Funding: This research was funded by the Zhejiang Provincial Natural Science Foundation of China under grant no. LY19B060009 and National Key Research and Development Project of China (2019YFC0214504). The authors also gratefully acknowledge the financial support from the State Key Laboratory of Green Chemistry Synthesis Technology (GCST-20200006).

Conflicts of Interest: The authors declare no conflict of interest. The funders had no role in the design of the study; in the collection, analyses, or interpretation of data; in the writing of the manuscript, or in the decision to publish the results.

References

1. Ameduri, B. From Vinylidene Fluoride (VDF) to the Applications of VDF-Containing Polymers and Copolymers: Recent Developments and Future Trends. *Chem. Rev.* **2009**, *109*, 6632–6686. [[CrossRef](#)]
2. Li, D.H.; Qi, S.C.; Zhang, X.A.; Liao, M.Y. Preparation, Functionalization and Properties of Low Molecular Fluoropolymers. *Prog. Chem.* **2016**, *28*, 673–685. [[CrossRef](#)]
3. Stadlober, B.; Zirkel, M.; Irimia-Vladu, M. Route towards sustainable smart sensors: Ferroelectric polyvinylidene fluoride-based materials and their integration in flexible electronics. *Chem. Soc. Rev.* **2019**, *48*, 1787–1825. [[CrossRef](#)]
4. Hu, X.P.; Che, Y.P.; Zhang, Z.J.; Shen, Q.D.; Chu, B.J. BiFeO₃-BaTiO₃/P(VDF-TrFE) Multifunctional Polymer Nanocomposites. *ACS Appl. Electron. Mater.* **2021**, *3*, 743–751. [[CrossRef](#)]
5. Yang, J.F.; Zhang, H.R.; Zhou, Q.; Qu, H.T.; Dong, T.T.; Zhang, M.; Tang, B.; Zhang, J.J.; Cui, G.L. Safety-Enhanced Polymer Electrolytes for Sodium Batteries: Recent Progress and Perspectives. *ACS Appl. Mater. Interfaces* **2019**, *11*, 17109–17127. [[CrossRef](#)]
6. Han, W.; Zhang, C.; Wang, H.; Zhou, S.; Tang, H.; Yang, L.; Wang, Z. Sub-nano MgF₂ embedded in carbon nanofibers and electrospun MgF₂ nanofibers by one-step electrospinning as highly efficient catalysts for 1,1,1-trifluoroethane dehydrofluorination. *Catal. Sci. Technol.* **2017**, *7*, 6000–6012. [[CrossRef](#)]
7. Cheng, Y.M.; Wang, J.C.; Han, W.F.; Song, Y.Y.; Liu, W.C.; Yang, L.T.; Wang, S.C.; Wu, Z.X.; Tang, H.D.; Zhang, J.J.; et al. Catalytic coupling of CH₄ with CHF₃ for the synthesis of VDF over LaOF catalyst. *Greenh. Gases* **2018**, *8*, 587–602. [[CrossRef](#)]
8. Han, W.; Song, Y.; Liu, W.; Yang, L.; Tang, H.; Wang, S.; Wu, Z.; Zhang, J. Promotion of O₂ on the co-pyrolysis of CHF₃ and CH₄ for VDF synthesis. *Greenh. Gases Sci. Technol.* **2017**, *7*, 891–902. [[CrossRef](#)]
9. Han, W.; Li, Y.; Tang, H.; Liu, H. Treatment of the potent greenhouse gas, CHF₃—An overview. *J. Fluor. Chem.* **2012**, *140*, 7–16. [[CrossRef](#)]
10. Han, W.F.; Kennedy, E.M.; Mackie, J.C.; Dlugogorski, B.Z. Synthesis of Vinylidene Fluoride via Reaction of Chlorodifluoromethane (HCFC-22) with Methane. *Ind. Eng. Chem. Res.* **2010**, *49*, 6010–6019. [[CrossRef](#)]
11. Chen, C.; Shen, Z.B.; Zhu, Y.P.; Wang, F.; Jiang, B.; Qi, H.M. Construction of activated carbon-supported B₃N₃ doped carbon as metal-free catalyst for dehydrochlorination of 1,2-dichloroethane to produce vinyl chloride. *RSC Adv.* **2021**, *11*, 183–191. [[CrossRef](#)]
12. Zhang, P.Z.; Jiang, Z.B.; Cui, Y.H.; Xie, G.Q.; Jin, Y.Z.; Guo, L.L.; Xu, Y.Q.; Zhang, Q.F.; Li, X.N. Catalytic performance of ionic liquid for dehydrochlorination reaction: Excellent activity and unparalleled stability. *Appl. Catal. B* **2019**, *255*, 117757. [[CrossRef](#)]
13. Tian, S.; Mao, W.; Sun, P.F.; Dang, J.S.; Zhou, L.; Lu, J.; Kemnitz, E. Breakthrough synthesis of 2,3,3,3-tetrafluoropropene via hydrogen-assisted selective dehydrochlorination of 1,1,1,2-tetrafluoro-2-chloropropane over nickel phosphides. *J. Catal.* **2020**, *391*, 366–377. [[CrossRef](#)]
14. Yuan, J.J.; Hong, Z.; Xi, Z.W.; Jia, W.Z.; Huang, Z.; Li, J.H.; Zhu, Z.R. Catalytic Pyrolysis of 2-Chloro-1,1-difluoroethane to Synthesize Vinylidene Fluoride over the Potassium-Promoted Carbon Catalysts. *ChemistrySelect* **2020**, *5*, 5788–5793. [[CrossRef](#)]
15. Wang, Z.K.; Han, W.F.; Zhang, C.P.; Zhou, S.L.; Wang, H.L.; Tang, H.D.; Liu, H.Z. Preparation of N-Doped Activated Carbon for Catalytic Pyrolysis of 1-Chloro-1,1-difluoroethane to Vinylidene Fluoride. *ChemistrySelect* **2018**, *3*, 1015–1018. [[CrossRef](#)]
16. Wang, Z.K.; Han, W.F.; Tang, H.D.; Li, Y.; Liu, H.Z. Preparation of N-doped ordered mesoporous carbon and catalytic performance for the pyrolysis of 1-chloro-1,1-difluoroethane to vinylidene fluoride. *Microporous Mesoporous Mat.* **2019**, *275*, 200–206. [[CrossRef](#)]
17. Han, W.F.; Liu, B.; Kang, Y.K.; Wang, Z.K.; Yu, W.; Yang, H.; Liu, Y.N.; Lu, J.Q.; Tang, H.D.; Li, Y.; et al. Experimental and DFT Mechanistic Study of Dehydrohalogenation of 1-Chloro-1,1-difluoroethane over Metal Fluorides. *Ind. Eng. Chem. Res.* **2019**, *58*, 18149–18159. [[CrossRef](#)]
18. Liu, W.C.; Liu, Y.N.; Mardochee, K.M.; Wang, Z.K.; Wang, S.C.; Yu, W.; Zhang, J.J.; Han, W.F. Selectivity Dependence of 1,1-Difluoro-1-Chloroethane Dehydrohalogenation on the Metal-Support Interaction over SrF₂ Catalyst. *Catalysts* **2020**, *10*, 355. [[CrossRef](#)]
19. Wang, Z.K.; Han, W.F.; Liu, H.Z. EDTA-assisted hydrothermal synthesis of cubic SrF₂ particles and their catalytic performance for the pyrolysis of 1-chloro-1,1-difluoroethane to vinylidene fluoride. *CrystEngComm* **2019**, *21*, 1691–1700. [[CrossRef](#)]
20. Wang, Z.K.; Han, W.F.; Tang, H.D.; Liu, H.Z. CaBaF_x composite as robust catalyst for the pyrolysis of 1-chloro-1,1-difluoroethane to vinylidene fluoride. *Catal. Commun.* **2019**, *120*, 42–45. [[CrossRef](#)]
21. Yu, W.; Han, W.F.; Liu, Y.N.; Lu, J.Q.; Yang, H.; Liu, B.; Tang, H.D.; Chen, A.M.; Li, Y. Facile Preparation of BaCl_xF_y for the Catalytic Dehydrochlorination of 1-Chloro-1,1-Difluoroethane to Vinylidene Fluoride. *Catalysts* **2020**, *10*, 377. [[CrossRef](#)]
22. Breitfeld, S.; Scholz, G.; Emmerling, F.; Kemnitz, E. BaF-benzenedicarboxylate: The first mechanochemical synthesis of a new coordination polymer with a direct Ba-F bond. *J. Mater. Sci.* **2018**, *53*, 13682–13689. [[CrossRef](#)]

-
23. Gauzzi, A.; Mathieu, H.J.; James, J.H.; Kellett, B. AES, XPS and SIMS characterization of $\text{YBa}_2\text{Cu}_3\text{O}_7$ superconducting high- T_c thin-films. *Vacuum* **1990**, *41*, 870–874. [[CrossRef](#)]
 24. He, K.; Chen, N.; Wang, C.; Wei, L.; Chen, J. Method for Determining Crystal Grain Size by X-Ray Diffraction. *Cryst. Res. Technol.* **2018**, *53*, 1700157. [[CrossRef](#)]